Construction of transcript regulation mechanism prediction models based on binding motif environment of transcription factor AoXlnR in *Aspergillus oryzae*

Hiroya Oka[1], Takaaki Kojima[1*], Ryuji Kato[2], Kunio Ihara[3], Hideo Nakano[1]

[1]Department of Applied Biosciences, Graduate School of Bioagricultural Sciences, Nagoya University, Furo-cho, Chikusa-ku, Nagoya 464-8601, Japan

[2]Graduate School of Pharmaceutical Sciences, Nagoya University, Furo-cho, Chikusa-ku, Nagoya 464-8601, Japan

[3]Center for Gene Research, Nagoya University, Furo-cho, Chikusa-ku, Nagoya 464-8602, Japan

*To whom correspondence should be addressed. Tel: +81 52 789 4144; Fax: +81 52 789 4145; E-mail: kojimat@agr.nagoya-u.ac.jp

Abstract

Recent study revealed that there are thousands of genes that remain unaffected by increased AoXlnR expression, despite the presence of one or more AoXlnR-binding motifs in their promoter region. Given this knowledge, we designed this study to construct several predictive models for determining whether a gene can exhibit a differential response to changes in AoXlnR expression. These models were constructed using 3D DNA shape information determined using the sequence around the AoXlnR binding motifs with classification as functional or nonfunctional. These models were created using a support vector machine followed by the evaluations designed to determine whether these DNA shape-based models can correctly classify functional motifs in terms of area under the receiver operating characteristic curve. The results showed that the differential expression levels of genes located downstream of the AoXlnR motif are closely related to specific DNA shape information around the binding motifs. Furthermore, we found that the parameters contributing to differential expressions differed depending on the number of motifs in the promoter region by comparing the prediction models using regions with only one binding DNA motif and those with multiple binding DNA motifs.

Author Summary

DNA-binding transcription factors (TFs) play a central role in transcriptional regulation mechanisms, mainly through their specific binding to target sites on the genome and regulation of the expression of downstream genes. Therefore, a comprehensive analysis of the function of these TFs will lead to the understanding of various biological mechanisms. However, the functions of TFs *in vivo* are diverse and complicated, and the identified binding sites on the genome are not necessarily involved in the regulation of downstream gene expression. In this study, we investigated whether DNA structural information around the binding site of transcription factors can be used to predict the involvement of the binding site in the regulation of the expression of genes located downstream of the binding site. Specifically, we calculated the structural parameters based on the DNA shape around the DNA binding motif located upstream of the gene whose expression is directly regulated by the transcription factor AoXlnR from *Aspergillus oryzae*, and showed that the presence or absence of expression regulation can be predicted from the sequence information with high accuracy by machine learning incorporating these parameters.

Introduction

Transcription factors (TFs) play a central role in complicated and diverse transcriptional regulatory mechanisms [1], therefore, the comprehensive analysis of the functions of TFs is critical to our understanding of various biological mechanisms. TF-DNA interactions have been analyzed by SELEX-Seq [2, 3], ChIP-Seq [4], whereas the effect of TFs on the expression of genes has been mostly evaluated by RNA-Seq and microarray. In order to comprehensively understand complicated regulatory mechanisms mediated by TFs, it is necessary to integrate several biological information acquired by these different techniques for comprehensive visualization of transcriptional regulatory mechanisms [5-7].

The binding preference of a TF is generally expressed as a DNA motif with 10 to 20 bp in length allowing a variety of sequence substitutions. The binding motifs can be analyzed from the collected TF-binding sequences using the position weight matrix (PWM) that calculates the probability of a base appearing at one sequential position independently, followed by the visualization of the probability as a motif logo. However, PWM does not consider interactions between adjacent sequences [8, 9]. Additionally, several studies have shown that the number of TF binding sites intrinsically related to the expression of these regulated genes in cells is significantly less than that of the binding DNA motifs in the genome [10, 11], which suggests the need for developing an alternative, more multifaceted, approach to understand the complex relationship between TFs and their binding sites.

Olson and co-workers first analyzed the crystal structures of complex of various 10 bp DNA double strand and a TF, and determined DNA shape parameters from the calculated average structurers of the DNA-TF complexes [12]. Later, four parameters, HelT, MGW, ProT, and Roll were developed as DNA shape features by Zhou and co-workers using a pentamer-based modelling from all-atom Monte Carlo simulations of DNA structures [13]. A recent study using these parameters showed that recognition sequences of more than 100 TFs were determined by the DNA shape information more accurately than by conventional sequence-based methods, indicating that PWMs ignore the conformational aspects of DNA in TF binding [14]. Additionally, several studies have reported that the inclusion of the DNA shape information enhanced the accuracy of TF-binding prediction models constructed only from DNA sequence information [15, 16]. For example, Dror *et al*. showed that DNA conformational preferences differ between TF families by evaluating DNA shape information around TF-binding sites [17]. However, to date, these studies have primarily focused on only

91 the difference among TF family units, such as C2H2 zinc finger TFs, not on an
92 individual TF. Additionally, no in-depth analysis linking TF preference, DNA shape
93 and regulatory gene expression has yet been reported for most individual TFs, except
94 for one paper [7].
95 In our previous study, we used integrated experimental data obtained from
96 genomic SELEX-Seq (gSELEX-Seq) and microarray analysis [5, 6] to evaluate all
97 genes transcriptionally regulated by the *Aspergillus oryzae* TF AoXlnR. *In vitro*
98 AoXlnR binding sites were detected in the promoter regions of more than 2000 genes,
99 however, less than 3% of these genes responded to high expression of AoXlnR in *A.*
100 *oryzae* cells [6]. This result strongly indicates the existence of an unknown factor
101 regulating TF-DNA interaction in addition to the targeted DNA sequences.
102 In this study, by using gSELEX-Seq and DNA micro array data of AoXlnR
103 used in a previous study [6], we constructed predictive models with a support vector
104 machine to investigate the relationship between the conformations of DNA around the
105 TF-binding motifs for AoXlnR and the expression of downstream genes (Fig. 1). The
106 results of these evaluations showed that AoXlnR-regulated differential expression could
107 be predicted with high accuracy using the DNA shape parameters of the sequence
108 surrounding TF-binding motifs. Furthermore, it was confirmed that the optimal model
109 for predicting the differential expression depends on the number of binding motifs in the
110 promoter region.
111

Results

Construction of AoXlnR binding motif classification models using DNA shape parameters

We identified 51 genes likely to be directly regulated by AoXlnR by integrating information of the binding sites in *A. oryzae* genome obtained from gSELEX-Seq [6] and the differential expression data obtained from the microarray completed in a previous study [18]. The 194 DNA shape parameters (MGW:48, ProT:48, HelT:49, and Roll:49) were used as explanatory valuables for constructing classifying AoXlnR binding motifs as MPD (63 motifs) or MPnD (1506 motifs). Model performances were evaluated with their AUC values (Fig. 2, Supplementary Fig 1). AUC for the model constructed with selected DNA shape parameters was higher than those for the models that used all the parameters. The selection of contributed DNA shape parameters improved the performance of the prediction. When the same procedure was applied to construct models using the antisense sequences of the AoXlnR binding motifs, the obtained performances using selected shape features were significantly higher than that using all shape features was the case with the original AoXlnR-binding motif sequences (Fig. 2, Supplementary Fig. 1).

Stratification of differential expression prediction models based on the number of binding motifs in promoters

The number of recognition sequences in a promoter was suggested to be associated with its responsiveness to that TF previously [6]. Therefore, we stratified MPDs according to the number of AoXlnR motifs present in their promoter regions, separating them into two groups: one motif and two or more motifs.

The DNA shape parameters of the classified datasets were calculated and then used to produce the prediction models as described above. When these models were compared, we found that the models constructed using the top parameters with the highest contribution to the expression differences showed significantly higher AUC values than the models constructed using all the parameters, as in the case of using the non-stratified MPDs (Fig. 3, Supplementary Fig. 2). Additionally, the model constructed using the stratified dataset showed higher AUC values than those constructed using the unclassified datasets. In particular, the classification by the number of motifs tended to more highly contribute to increased AUC values when analyzing the antisense sequences of the AoXlnR binding motifs (Figs. 3B, D, F and H, Supplementary Figs. 2B and 2D).

149 **Discussion**

150 This study was designed to evaluate the underlying mechanisms regulating
151 gene expression in response to *A. oryzae* TF, AoXlnR, from the viewpoint of DNA
152 conformation around the binding sites. We used datasets containing information on the
153 binding sites of AoXlnR in the *A. oryzae* genome and their differential expression in
154 response to the overexpression of this TF to construct mathematical models explaining
155 the differential regulation of AoXlnR binding sites [6, 18].

156 We first determined the impact of each of the 194 parameters for each AoXlnR
157 recognition region using 3D DNA shape information. These values were then used to
158 construct individual prediction models, followed by applying to predict responsiveness
159 to this TF. However, the AUCs of the models constructed using SVM were 0.644 and
160 0.522 for the sense and antisense strand sides, respectively, indicating that the accuracy
161 of the constructed models was insufficient to reliably distinguish between DEG and
162 non-DEG promoters (Fig. 2, Supplementary Fig. 1). These results suggest that the
163 inclusion of parameters with small contribution to the differential expressions via
164 AoXlnR prevented the construction of accurate prediction models.

165 Thus, we selected the top parameters in the order of their coefficient
166 contributing to the discrimination of differential expression to reduce the number of
167 explanatory variables used in the prediction models. These models were then
168 reconstructed using two to ten selected parameters. These models displayed AUCs of
169 more than 0.7 marking a significant improvement compared to the above models using
170 all parameters (Fig. 2, Supplementary Fig. 1). It should be noted that certain DNA
171 structural parameters were included in most of the models with higher AUCs. In fact,
172 one of the parameters, down_17_ProT, that is determined by the sequences around 17 b
173 downstream of the AoXlnR binding motifs, was preferentially selected. In the case of
174 model construction using the antisense strand of the motif, the DNA shape parameters
175 related to 15 b upstream of the binding motifs were observed at a relatively high
176 frequency. These preferentially selected parameters were calculated from the structure
177 of sequences outside of the conventional binding motif sequences, 5'-GGCTGA-3' or 5'-
178 GGCTAA-3'. This fact strongly suggests the existence of a regulatory mechanism for
179 the expression of AoXlnR, which has not been revealed by conventional analyses based
180 only on TF-binding motif information. We are currently planning to introduce
181 mutations in the promoter region to alter the down_17_ProT parameters to understand
182 how this impacts gene regulation.

183 Next, we further classified the MPDs by the presence of other motifs in the
184 same promoter region, and then subjected the classified dataset to the construction of a

185 new set of models, followed by the evaluation of the performance of resultant models.
186 The results demonstrated that models constructed using the selected parameters which
187 contributed to the model performance showed higher AUC than the models constructed
188 under conditions with no classification by the number of motifs, including those using
189 antisense strands (Figs. 3, Supplementary Fig. 2). We also randomly stratified the
190 dataset including DNA shape parameters of MPD to validate the effect of stratification
191 by the number of models on the accuracy of the model. Although the randomly
192 stratified prediction models showed also high values with that of the model constructed
193 according to the motif of the sense strands, the models based on the antisense strands of
194 binding motifs showed higher AUC than that of the randomly stratified prediction
195 models (Supplementary Fig. 3). Furthermore, preferentially selected parameters were
196 different compared to the model using MPDs from the promoters including multiple
197 motifs (Supplementary Fig. 4). For example, the models based on multiple parameters
198 selected up_17_Roll, up_7_Roll and up_19_Roll as the highly contributed parameters,
199 whereas the randomly stratified model selected up_19_Roll, down_20_down and
200 down_15_MGW. These results imply that different parameters contribute to the
201 differential expressions depending on the number of binding motifs in the promoter.
202 In the models based on the DNA shape parameters around the binding motifs in
203 promoters of sense strand including only one motif, down_23_ProT was preferentially
204 selected as in all MPD-based models (Supplementary Fig. 2A), while up_17_Roll was
205 preferentially selected in the models produced for promoter with several binding motifs
206 (Supplementary Fig. 2C). In contrast, the models produced using the antisense strand
207 showed a preference for up_17_ProT or up_11_HelT where the models were
208 constructed for single or multiple motif entries, respectively (Supplementary Figs. 2B
209 and D). The difference in the preferred DNA shape parameters among these models
210 resulted in improved AUCs, suggesting that the regulatory mechanism of AoXlnR in
211 cells depends on the number of motifs in the promoter region.
212 Interestingly, *xynF1* (AO090103000423), which is known to be under the
213 control of AoXlnR [21], was more accurately discriminated as a gene regulated by
214 AoXlnR when the sequence around the MPD in the promoter was evaluated using
215 models constructed from MPDs with multiple motifs (100%) compared to the models
216 without classification (10%). On the other hand, randomly classified models provided
217 around 50% of *xynF1*'s correct discrimination rate, which is much lower than that of the
218 models using dataset of MPDs with multiple motifs (data not shown). Taken together,
219 these results suggest that the mechanisms of expression regulation by AoXlnR in cells
220 can be classified by the number and orientation of the AoXlnR binding motifs.

The DNA shape information used in this study was recently reported to play an important role in TF-DNA interactions [14, 22, 23]. These reports focus on the relationship between TF-DNA interactions and the DNA structure around the binding sites. Based on these approaches, we examined whether it is possible to distinguish between TF-DNA interactions observed only in *in vitro* binding reactions and TF-DNA interactions in which TF binds linked to its gene regulation in cells and are presumed to regulate the expression of downstream genes, in terms of the DNA structure around the binding sites. Our results showed that some of the structural parameters calculated from DNA sequences around the AoXlnR binding sites were closely related to the differential expression of the regulatory genes in the cell as well as in *in vitro* binding between AoXlnR and its target binding sites.

In *Aspergillus oryzae*, a paralogous TF of AoXlnR, AraR regulates similar genes involved in the catabolism pentose pathway. Although AraR and AoXlnR are similar, their target genes and target sequences are slightly different. In 2018, Ishikawa et al. reported that these TFs demonstrate no cooperative binding, but do display competitive bindings at their shared sites [24]. Therefore, the existence of AraR binding may influence the DNA conformation of AoXlnR binding sites in specific genes.

Li *et al*. reported nine additional DNA shape parameters, including four inter-bp or bp-step parameters (Rise, Shift, Slide, and Tilt) and five intra-bp or bp parameters (Buckle, Opening Shear, Stagger, and Stretch) in 2017 [25]. The construction of models for predicting the differential expression with improved accuracy may be accomplished by adding these nine parameters to the four structural parameters used in this study.

Furthermore, our models have no consideration of any other factors involved in transcriptional regulation, including chromatin accessibility, and cytosine methylation. For example, chromatin condensation forms heterochromatin and prevents TFs from binding to their preferred sequences [26, 27]. By adding the information of such epigenetic modifications as new parameters, more accurate model can be constructed for the regulatory mechanisms of various TFs, including AoXlnR.

Materials and Methods

Calculating the structural parameters for the regions surrounding the AoXlnR-binding motifs using DNA shape parameters

In our previous study, we divided the set of detected genes of *A. oryzae* into two groups based on their differential expression in response to over-expression of AoXlnR: 1) genes that retain one or more AoXlnR-binding sites in their promoter regions and are expression-responsive to AoXlnR and 2) genes that retain AoXlnR binding sites in the promoter regions but were not sensitive to AoXlnR overexpression [6]. Considering the binding profile of AoXlnR, in which AoXlnR preferentially binds to 5'-GGCT(G/A)A-3' [6, 18], the number and position of 5'-GGCTGA-3' or 5'-GGCTAA-3' motif were obtained from 1000 bp upstream of the start codon of genes in *A.oryzae*, generating 50 b sequences that include the AoXlnR binding motif and both sides of adjacent 22 b sequences. Here we refer to the binding motifs from the promoters of genes that are responsive to overexpression as "Motif in the Promoter region of DEGs" (MPD) and motifs in the promoters of genes unresponsive to overexpression as "Motif in the Promoter region of non-DEGs" (MPnD). Note that the binding motif closest to the start codon was selected when multiple motifs were present in the promoter region.

We then calculated the DNA shape parameters (HelT, MGW, ProT, and Roll values) for each of these 50 b sequences using the DNAshapeR package from R (version 1.16.0; https://bioconductor.org/packages/release/bioc/html/DNAshapeR.html), which uses a pentamer-based prediction model built from all-atom Monte Carlo simulations of DNA structures [13, 19]. The resulting dataset contained 194 parameter values (MGW:48, ProT:48, HelT:49, and Roll:49), including the mean and standard deviation over all positions [20] for every 50 b unit around 63 MPDs (Sense strand 34 and Antisense strand 29, Table 1) and 1506 MPnDs (Supplementary Tables 1 and 2).

Table 1. The number of AoXlnR binding motif in the promoter of MPDs.

Gene ID	GGCTGA number	GGCTAA number	Sense sum	Sense presence	TCAGCC number	TTAGCC number	Antisense sum	Antisense presence
AO090120000026	1	1	2	1	1	1	2	1
AO090011000140	0	1	1	1	0	3	3	1
AO090005000986	1	1	2	1	1	0	1	1
AO090001000649	0	1	1	1	0	2	2	1
AO090003000859	0	0	0	0	1	2	3	1
AO090103000423	1	1	2	1	0	0	0	0

AO090005000698	0	1	1	1	1	0	1	1
AO090001000208	1	0	1	1	0	1	1	1
AO090001000111	0	0	0	0	0	0	0	0
AO090003001277	0	0	0	0	2	2	4	1
AO090003000782	0	2	2	1	0	0	0	0
AO090001000069	0	1	1	1	2	0	2	1
AO090011000483	0	1	1	1	0	0	0	0
AO090010000063	0	0	0	0	0	1	1	1
AO090011000141	1	3	4	1	0	1	1	1
AO090701000885	2	0	2	1	0	1	1	1
AO090001000267	0	2	2	1	0	0	0	0
AO090701000345	0	0	0	0	0	2	2	1
AO090020000603	0	0	0	0	1	1	2	1
AO090023000401	1	0	1	1	0	0	0	0
AO090026000127	0	1	1	1	0	0	0	0
AO090102000040	0	1	1	1	0	0	0	0
AO090003001484	0	1	1	1	0	0	0	0
AO090012000034	1	0	1	1	0	0	0	0
AO090020000042	0	0	0	0	0	1	1	1
AO090003000463	0	0	0	0	1	0	1	1
AO090701000886	0	0	0	0	0	0	0	0
AO090005000189	0	0	0	0	0	0	0	0
AO090701000274	0	1	1	1	1	2	3	1
AO090023000787	2	0	2	1	0	1	1	1
AO090103000268	0	2	2	1	0	1	1	1
AO090701000639	0	2	2	1	0	0	0	0
AO090010000314	0	2	2	1	0	0	0	0
AO090012000445	0	2	2	1	0	0	0	0
AO090103000087	0	1	1	1	0	1	1	1
AO090005000337	0	1	1	1	0	0	0	0
AO090026000102	1	0	1	1	0	0	0	0
AO090005000423	0	0	0	0	1	0	1	1
AO090010000515	0	0	0	0	0	1	1	1
AO090011000745	0	1	1	1	2	1	3	1
AO090701000884	1	0	1	1	1	1	2	1
AO090001000207	0	1	1	1	0	1	1	1
AO090005000518	0	0	0	0	0	0	0	0
AO090003000905	1	0	1	1	0	2	2	1
AO090005001078	0	2	2	1	0	0	0	0
AO090103000426	0	1	1	1	0	1	1	1
AO090005001427	0	0	0	0	0	1	1	1
AO090038000631	0	0	0	0	0	0	0	0
AO090038000426	0	0	0	0	0	0	0	0
AO090001000348	1	0	1	1	0	1	1	1
AO090012000941	0	0	0	0	0	0	0	0
Total				34				29

Constructing models for predicting AoXlnR-dependent differential expression using a discriminant algorithm

We constructed a set of supervised learning models to predict whether AoXlnR-binding motifs, 5'-GGCT(G/A)A-3' in each gene promoter is in a DEG or non-DEG promoter region. The expression profiles of each of the 5'-GGCT(G/A)A-3' motif were determined using unpublished microarray analysis data of AoXlnR overexpression strain TFX2 and AoXlnR disruption strain SK253 conducted in a previous study [18]. In this study, we used a support vector machine (e1071 package; version 1.7-3; https://cran.r-project. org/web/packages/e1071) on R (version 4.0.1; https:// cran.ism.ac.jp/) as the binary classification algorithm.

To balance the difference in size between the number of MPD and MPnD, we selected the same number of MPnDs that showed the lowest response to AoXlnR overexpression as MPDs and synthesized a 50 b dataset consisting of the same number of MPDs and MPnDs. The expression variables, the DNA shape parameters were tagged with their labels; 1 for MPD, 0 for MPnD. The performance of prediction model was validated using leave-one-out cross validation. The area under the receiver operating characteristic curve (AUC) was used as the model evaluation criteria. These AUC values were calculated as the average from 10 sampling rounds.

The practical flow of building a prediction model is briefly described below (Fig. 1). First, two gene expression profiles were compared to make two categories of genes with AoXlnR-binding sites: the AoXlnR overexpression responsive genes, and AoXlnR overexpression non-responsive genes. Second, from the gene lists, the MPD and MPnD was searched. Third, from each MPD or MPnD, their sequence data of 50 b was converted into the DNA shape parameters using DNAshapeR. Fourth, using these datasets, model for predicting MPD or MPnD was constructed. In the construction of prediction model, the DNA shape parameters that significantly contribute to the differential expression of genes with the AoXlnR were ranked by calculating parameter coefficients from the SVM linear kernel, and selected parameters with a higher coefficient. Those prediction models were constructed using either (a) all DNA structure parameters, or 2 to 10 selected parameters (2 to 10 parameters) in the order of their coefficient (Supplementary Fig 1). Additionally, we constructed and evaluated a set of predictive models using datasets where MPD and MPnD data were further stratified on the number of motifs per promoter, i.e., one or more than one, using the same procedure described above. In parallel, we randomly stratified the dataset including DNA shape

parameters of MPD as the same procedure with the preparation of the stratified dataset considering the number of motifs. These randomly stratified dataset was used to construct prediction models (Supplementary Fig. 2).

Acknowledgments

We thank Tetsuo Kobayashi of Nagoya University for providing the microarray analysis data. This work was supported in part by JSPS KAKENHI Grant-in-Aid for Scientific Research(C) (Grant Number JP19K05766), JSPS KAKENHI Grant-in-Aid for JSPS fellow (Grant Number JP20J15715). This work was also financially supported in part by Mizutani Scholarship.

References

1. Todeschini AL, Georges A, Veitia RA. Transcription factors: specific DNA binding and specific gene regulation. Trends in Genetics. 2014;30(6):211-9. doi: 10.1016/j.tig.2014.04.002. PubMed PMID: WOS:000337266500001.

2. Zykovich A, Korf I, Segal DJ. Bind-n-Seq: high-throughput analysis of in vitro protein-DNA interactions using massively parallel sequencing. Nucleic Acids Research. 2009;37(22). doi: 10.1093/nar/gkp802. PubMed PMID: WOS:000272935000007.

3. Jolma A, Kivioja T, Toivonen J, Cheng L, Wei G, Enge M, et al. Multiplexed massively parallel SELEX for characterization of human transcription factor binding specificities. Genome Research. 2010;20(6):861-73. doi: 10.1101/gr.100552.109. PubMed PMID: WOS:000278269400016.

4. Johnson DS, Mortazavi A, Myers RM, Wold B. Genome-wide mapping of in vivo protein-DNA interactions. Science. 2007;316(5830):1497-502. doi: 10.1126/science.1141319. PubMed PMID: WOS:000247066400049.

5. Kojima T, Kunitake E, Ihara K, Kobayashi T, Nakano H. A Robust Analytical Pipeline for Genome-Wide Identification of the Genes Regulated by a Transcription Factor: Combinatorial Analysis Performed Using gSELEX-Seq and RNA-Seq. Plos One. 2016;11(7):16. doi: 10.1371/journal.pone.0159011. PubMed PMID: WOS:000379508300048.

6. Oka H, Kojima T, Ihara K, Kobayashi T, Nakano H. Comprehensive investigation of the gene expression system regulated by an Aspergillus oryzae transcription factor XlnR using integrated mining of gSELEX-Seq and microarray data. Bmc Genomics. 2019;20:10. doi: 10.1186/s12864-018-5375-5. PubMed PMID: WOS:000455209300002.

7. Kribelbauer JF, Loker RE, Feng SQ, Rastogi C, Abe N, Rube HT, et al. Context-Dependent Gene Regulation by Homeodomain Transcription Factor Complexes Revealed by Shape-Readout Deficient Proteins. Molecular Cell. 2020;78(1):152-+. doi: 10.1016/j.molcel.2020.01.027. PubMed PMID: WOS:000523321100014.

8. Eggeling R, Roos T, Myllymaki P, Grosse I. Inferring intra-motif dependencies of DNA binding sites from ChIP-seq data. Bmc Bioinformatics. 2015;16:15. doi: 10.1186/s12859-015-0797-4. PubMed PMID: WOS:000364458100002.

9. Wang J, Zhuang J, Iyer S, Lin X, Whitfield TW, Greven MC, et al. Sequence features and chromatin structure around the genomic regions bound by 119 human transcription factors. Genome Research. 2012;22(9):1798-812. doi: 10.1101/gr.139105.112. PubMed PMID: WOS:000308272800020.

10. Landolin JM, Johnson DS, Trinklein ND, Aldred SF, Medina C, Shulha H, et al. Sequence features that drive human promoter function and tissue specificity. Genome Research. 2010;20(7):890-8. doi: 10.1101/gr.100370.109. PubMed PMID: WOS:000279404700003.

11. Spitz F, Furlong EEM. Transcription factors: from enhancer binding to developmental

control. Nature Reviews Genetics. 2012;13(9):613-26. doi: 10.1038/nrg3207. PubMed PMID: WOS:000308064000009.

12. Olson WK, Gorin AA, Lu XJ, Hock LM, Zhurkin VB. DNA sequence-dependent deformability deduced from protein-DNA crystal complexes. Proceedings of the National Academy of Sciences of the United States of America. 1998;95(19):11163-8. doi: 10.1073/pnas.95.19.11163. PubMed PMID: WOS:000075957100030.

13. Zhou TY, Yang L, Lu Y, Dror I, Machado ACD, Ghane T, et al. DNAshape: a method for the high-throughput prediction of DNA structural features on a genomic scale. Nucleic Acids Research. 2013;41(W1):W56-W62. doi: 10.1093/nar/gkt437. PubMed PMID: WOS:000323603200010.

14. Samee MAH, Bruneau BG, Pollard KS. A De Novo Shape Motif Discovery Algorithm Reveals Preferences of Transcription Factors for DNA Shape Beyond Sequence Motifs. Cell Systems. 2019;8(1):27-+. doi: 10.1016/j.cels.2018.12.001. PubMed PMID: WOS:000456545100004.

15. Zhou TY, Shen N, Yang L, Abe N, Horton J, Mann RS, et al. Quantitative modeling of transcription factor binding specificities using DNA shape. Proceedings of the National Academy of Sciences of the United States of America. 2015;112(15):4654-9. doi: 10.1073/pnas.1422023112. PubMed PMID: WOS:000352856800049.

16. Chiu TP, Xin BB, Markarian N, Wang YF, Rohs R. TFBSshape: an expanded motif database for DNA shape features of transcription factor binding sites. Nucleic Acids Research. 2020;48(D1):D246-D55. doi: 10.1093/nar/gkz970. PubMed PMID: WOS:000525956700035.

17. Dror I, Golan T, Levy C, Rohs R, Mandel-Gutfreund Y. A widespread role of the motif environment in transcription factor binding across diverse protein families. Genome Research. 2015;25(9):1268-80. doi: 10.1101/gr.184671.114. PubMed PMID: WOS:000360721000003.

18. Noguchi Y, Sano M, Kanamaru K, Ko T, Takeuchi M, Kato M, et al. Genes regulated by AoXlnR, the xylanolytic and cellulolytic transcriptional regulator, in Aspergillus oryzae. Applied Microbiology and Biotechnology. 2009;85(1):141-54. doi: 10.1007/s00253-009-2236-9. PubMed PMID: WOS:000271025100014.

19. Chiu TP, Comoglio F, Zhou TY, Yang L, Paro R, Rohs R. DNAshapeR: an R/Bioconductor package for DNA shape prediction and feature encoding. Bioinformatics. 2016;32(8):1211-3. doi: 10.1093/bioinformatics/btv735. PubMed PMID: WOS:000374476800013.

20. Peng PC, Sinha S. Quantitative modeling of gene expression using DNA shape features of binding sites. Nucleic Acids Research. 2016;44(13):9. doi: 10.1093/nar/gkw446. PubMed PMID: WOS:000382999300005.

21. Kitamoto N, Yoshino S, Ito M, Kimura T, Ohmiya K, Tsukagoshi N. Repression of the expression of genes encoding xylanolytic enzymes in Aspergillus oryzae by introduction of multiple copies of the xynF1 promoter. Applied Microbiology and Biotechnology. 1998;50(5):558-63. doi: 10.1007/s002530051334. PubMed PMID: WOS:000077439900007.

402 22. Al-Zyoud WA, Hynson RMG, Ganuelas LA, Coster ACF, Duff AP, Baker MAB, et al.
403 Binding of transcription factor GabR to DNA requires recognition of DNA shape at a location distinct
404 from its cognate binding site. Nucleic Acids Research. 2016;44(3):1411-20. doi: 10.1093/nar/gkv1466.
405 PubMed PMID: WOS:000371268700042.
406 23. Wang XF, Zhou TY, Wunderlich Z, Maurano MT, DePace AH, Nuzhdin SV, et al. Analysis
407 of Genetic Variation Indicates DNA Shape Involvement in Purifying Selection. Molecular Biology
408 and Evolution. 2018;35(8):1958-67. doi: 10.1093/molbev/msy099. PubMed PMID:
409 WOS:000441143000010.
410 24. Ishikawa K, Kunitake E, Kawase T, Atsumi M, Noguchi Y, Ishikawa S, et al. Comparison
411 of the paralogous transcription factors AraR and XlnR in Aspergillus oryzae. Current Genetics.
412 2018;64(6):1245-60. doi: 10.1007/s00294-018-0837-5. PubMed PMID: WOS:000449259500011.
413 25. Li JS, Sagendorf JM, Chiu TP, Pasi M, Perez A, Rohs R. Expanding the repertoire of DNA
414 shape features for genome-scale studies of transcription factor binding. Nucleic Acids Research.
415 2017;45(22). doi: 10.1093/nar/gkx1145. PubMed PMID: WOS:000419064400028.
416 26. Song LY, Zhang ZC, Grasfeder LL, Boyle AP, Giresi PG, Lee BK, et al. Open chromatin
417 defined by DNaseI and FAIRE identifies regulatory elements that shape cell-type identity. Genome
418 Research. 2011;21(10):1757-67. doi: 10.1101/gr.121541.111. PubMed PMID:
419 WOS:000295407800019.
420 27. Xin BB, Rohs R. Relationship between histone modifications and transcription factor
421 binding is protein family specific. Genome Research. 2018;28(3):321-33. doi: 10.1101/gr.220079.116.
422 PubMed PMID: WOS:000426355600005.
423

424

425

426 **Figure Legends**

427 **Figure 1. Flowchart describing the construction of the supervised machine leaning**
428 **models to predict AoXlnR-dependent differential expression from DNA shape**
429 **parameters.**
430 The genes identified in previous studies were classified into two groups depending on
431 the detection method used in their isolation. The positions of AoXlnR binding motifs,
432 5'-GGCTGA-3' or 5'-GGCTAA-3' in each promoter of genes were investigated. Once
433 identified we extracted 22 b up and downstream of these recognition sites and used
434 these to identify the relevant DNA shape parameters. These parameters were then used
435 to construct the discriminative model used in the machine learning programs.
436

437 **Figure 2. ROC curves and box plots amongst the various models constructed using**
438 **DNA shape parameters.**
439 (A) ROC curve of the model based on the sense strands of MPDs.(B) ROC curve of the
440 model based on the antisense strands of MPDs.(C) Box plots of AUC values obtained
441 from ROC curve of the model based on the sense strands of MPDs.(D) Box plots of
442 AUC values obtained from ROC curve of the model based on the antisense strands of
443 MPDs. Each model was constructed using DNA shape parameters calculated from 50 b
444 sequences containing AoXlnR binding motifs. Here we displayed the ROC curves of the
445 models with the highest AUC for discriminant model using non-stratified MPDs
446 selected parameters shown in Supplementary Figure 1A (for the sense sequences) or 1B
447 (for the antisense sequences). The black lines show the ROCs of the model using all
448 DNA shape parameters, and the red lines show the ROCs of the model using only the
449 preferentially selected parameters shown in Supplementary Figure 1A or 1B. Ten lines
450 show the result of 10 times validation pairing the positive and negative samples in
451 LOOCV. The vertical axis of the ROC curve indicates the “Sensitivity", which is the
452 true positive rate, and the horizontal axis indicates the "1 - Specificity", which is the
453 false positive rate. p values were calculated using the Student’s t test. $*p < 0.05$.
454

455 **Figure 3. ROC curves and box plots amongst the various models constructed using**
456 **stratified dataset of DNA shape parameters.**
457 (A) ROC curve of the model based on the sense strands of MPDs from the promoters
458 including a single motif.(B) ROC curve of the model based on the antisense strands of
459 MPDs from the promoters including a single motif.(C) Box plots of AUC values
460 obtained from ROC curve of the model based on the sense strands of MPDs from the

promoters including a single motif.(D) Box plots of AUC values obtained from ROC curve of the model based on the antisense strands of MPDs from the promoters including a single motif.(E) ROC curve of the model based on the sense strands of MPDs from the promoters including multiple motifs.(F) ROC curve of the model based on the antisense strands of MPDs from the promoters including multiple motifs.(G) Box plots of AUC values obtained from ROC curve of the model based on the sense strands of MPDs from the promoters including multiple motifs.(H) Box plots of AUC values obtained from ROC curve of the model based on the antisense strands of MPDs from the promoters including multiple motifs. Each model was constructed using DNA shape parameters calculated from 50 b sequences containing AoXlnR binding motifs. Here we displayed the ROC curves of the models with the highest AUC for discriminant model using stratified MPDs selected parameters shown in Supplementary Figure 2A (for the sense sequences including a single motif), 2B (for the antisense sequences including a single motif), 2C (for the sense sequences including multiple motifs), or 2D (for the antisense sequences including multiple motifs). The black lines show the ROCs of the model using all DNA shape parameters, and the red lines show the ROCs of the model using only the preferentially selected parameters shown in Supplementary Figure 2. Ten lines show the result of 10 times validation pairing the positive and negative samples in LOOCV. The vertical axis of the ROC curve indicates the “Sensitivity", which is the true positive rate, and the horizontal axis indicates the "1 - Specificity", which is the false positive rate. p values were calculated using the Student’s t test. $*p < 0.05$.

483 **Supporting information captions**
484
485 **Supplementary Table 1. DNA shape parameter values of sense strand used in this**
486 **study.**
487
488 **Supplementary Table 2. DNA shape parameter values of anti-sense strand used in**
489 **this study.**
490
491 **Supplementary Figure 1. Parameters used and AUC values calculated in each**
492 **prediction model using non-stratified dataset of DNA shape parameters.**
493 Weight shows the contribution for each model. Black circle shows parameters used in
494 each model. The AUCs were calculated for models with 2 to 10 and all parameters. The
495 AUC surrounded by the red line is the highest AUC, and the model with the ROC curve
496 is shown in Fig. 2. (A) Models constructed based on binding motifs in sense strand. (B)
497 Models constructed based on binding motifs in antisense strand.
498
499 **Supplementary Figure 2. Parameters used and AUC values calculated in each**
500 **prediction model using stratified dataset of DNA shape parameters.**
501 Weight shows the contribution for each model. Black circle shows parameters used in
502 each model. The AUCs were calculated for models with 2 to 10 and all parameters. The
503 AUC surrounded by the red line is the highest AUC, and the model with the ROC curve
504 is shown in Fig. 3. (A) Models constructed based on single motifs in sense strand. (B)
505 Models constructed based on single motif in antisense strand. (C) Models constructed
506 based on multiple motifs in sense strand. (D) Models constructed based on multiple
507 motifs in antisense strand.
508
509 **Supplementary Figure 3. ROC curves and box plots amongst the various models**
510 **constructed using randomly stratified dataset of DNA shape parameters.**
511 (A) ROC curve of the model based on the sense strands of MPDs from the promoters
512 with same number of single motifs. (B) ROC curve of the model based on the antisense
513 strands of MPDs from the promoters with same number of single motifs. (C) Box plots
514 of AUC values obtained from ROC curve of the model based on the sense strands of
515 MPDs with same number of single motifs. (D) Box plots of AUC values obtained from
516 ROC curve of the model based on the antisense strands of MPDs with same number of
517 single motifs. (E) ROC curve of the model based on the sense strands of MPDs with
518 same number of multiple motifs. (F) ROC curve of the model based on the antisense

strands of MPDs with same number of multiple motifs. (G) Box plots of AUC values obtained from ROC curve of the model based on the sense strands of MPDs with same number of multiple motifs. (H) Box plots of AUC values obtained from ROC curve of the model based on the antisense strands of MPDs with same number of multiple motifs. Each model was constructed using DNA shape parameters calculated from 50 b sequences containing AoXlnR binding motifs. Here we displayed the ROC curves of the models with the highest AUC for discriminant model using stratified MPDs selected parameters shown in Supplementary Figure 4A (for the sense sequences including a single motif), 4B (for the antisense sequences including a single motif), 4C (for the sense sequences including multiple motifs), or 4D (for the antisense sequences including multiple motifs). The black lines show the ROCs of the model using all DNA shape parameters, and the red lines show the ROCs of the model using only the preferentially selected parameters shown in Supplementary Figure 4. Ten lines show the result of 10 times validation pairing the positive and negative samples in LOOCV. The vertical axis of the ROC curve indicates the “Sensitivity", which is the true positive rate, and the horizontal axis indicates the "1 - Specificity", which is the false positive rate. p values were calculated using the Student’s t test. $*p < 0.05$.

Supplementary Figure 4. Parameters used and AUC values calculated in each prediction model using randomly stratified dataset of DNA shape parameters. Weight shows the contribution for each model. Black circle shows parameters used in each model. The AUCs were calculated for models with 2 to 10 and all parameters. The AUC surrounded by the red line is the highest AUC, and the model with the ROC curve is shown in the Supplementary Figure 3. (A) Models constructed based on single motifs in sense strand. (B) Models constructed based on single motif in antisense strand. (C) Models constructed based on multiple motifs in sense strand. (D) Models constructed based on multiple motifs in antisense strand.

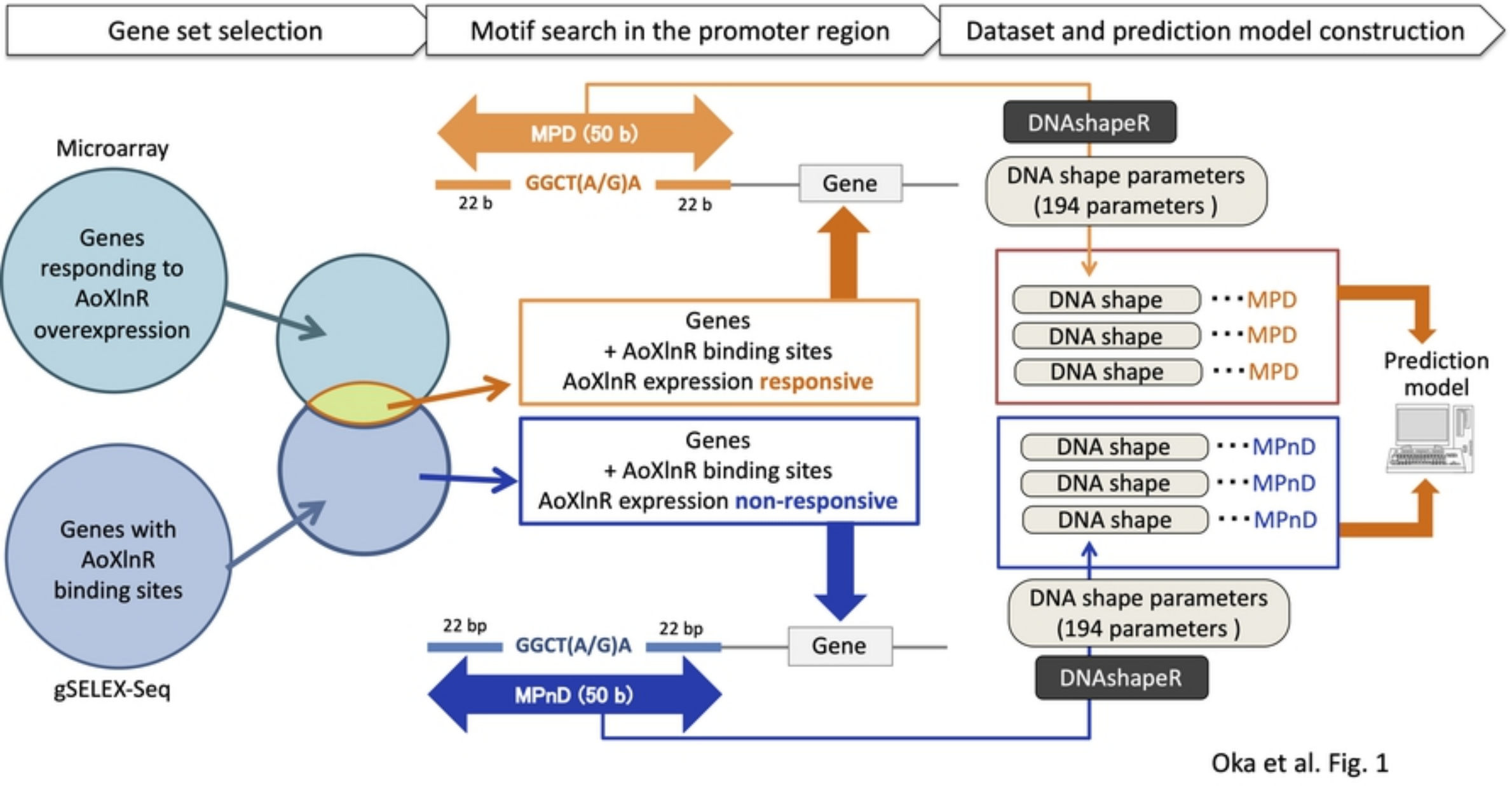
Gene set selection
Motif search in the promoter region
Dataset and prediction model construction
Microarray
Genes responding to AoXlnR overexpression
Genes with AoXlnR binding sites
gSELEX-Seq
MPD (50 b)
GGCT(A/G)A
22 b
22 b
Gene
Genes
+ AoXlnR binding sites
AoXlnR expression responsive
Genes
+ AoXlnR binding sites
AoXlnR expression non-responsive
22 bp
GGCT(A/G)A
22 bp
Gene
MPnD (50 b)
DNAshapeR
DNA shape parameters
(194 parameters)
DNA shape ···MPD
DNA shape ···MPD
DNA shape ···MPD
DNA shape ···MPnD
DNA shape ···MPnD
DNA shape ···MPnD
DNA shape parameters
(194 parameters)
DNAshapeR
Prediction model
Oka et al. Fig. 1

Figure

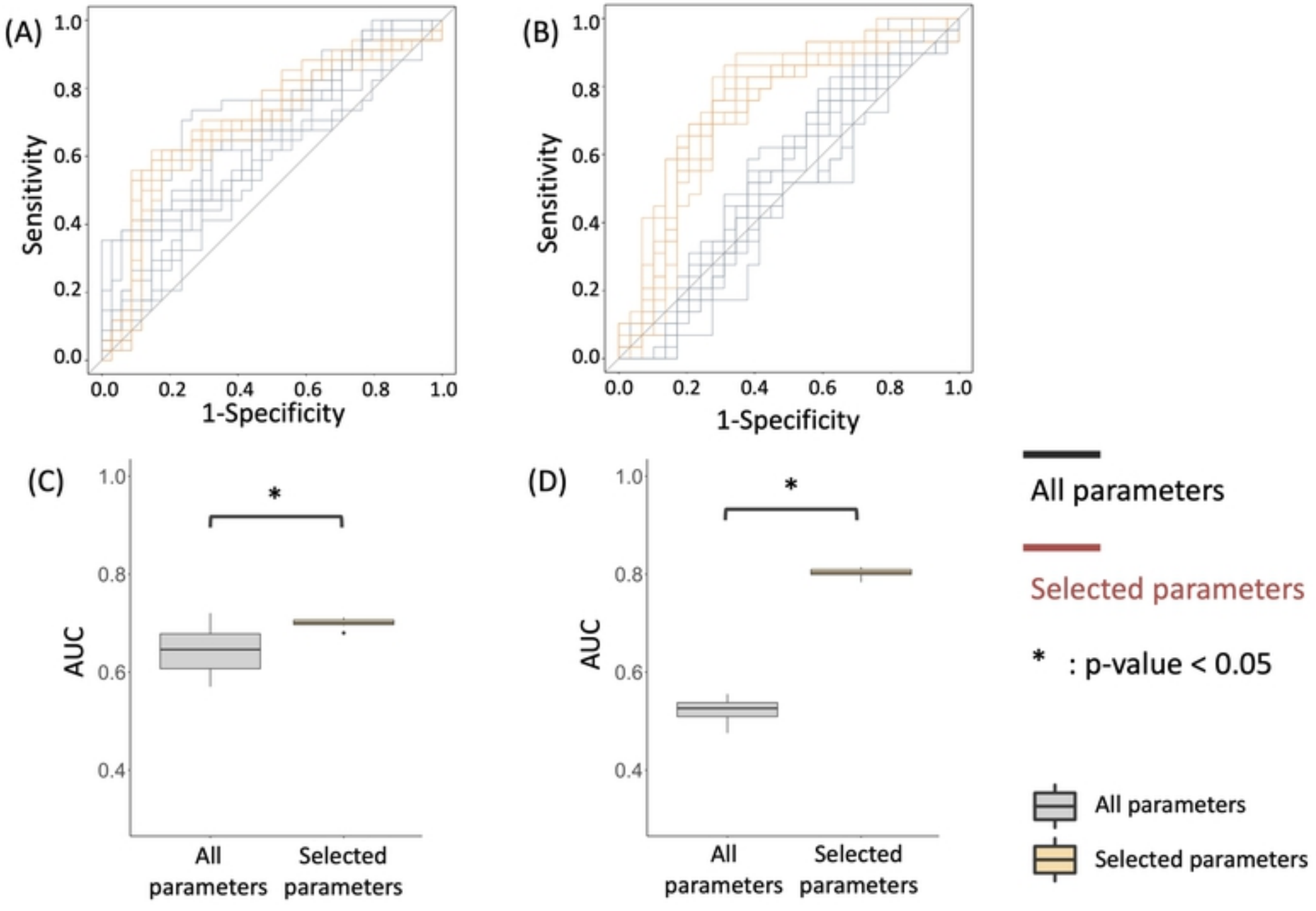

Oka et al. Figs. 2A to 2D

Figure

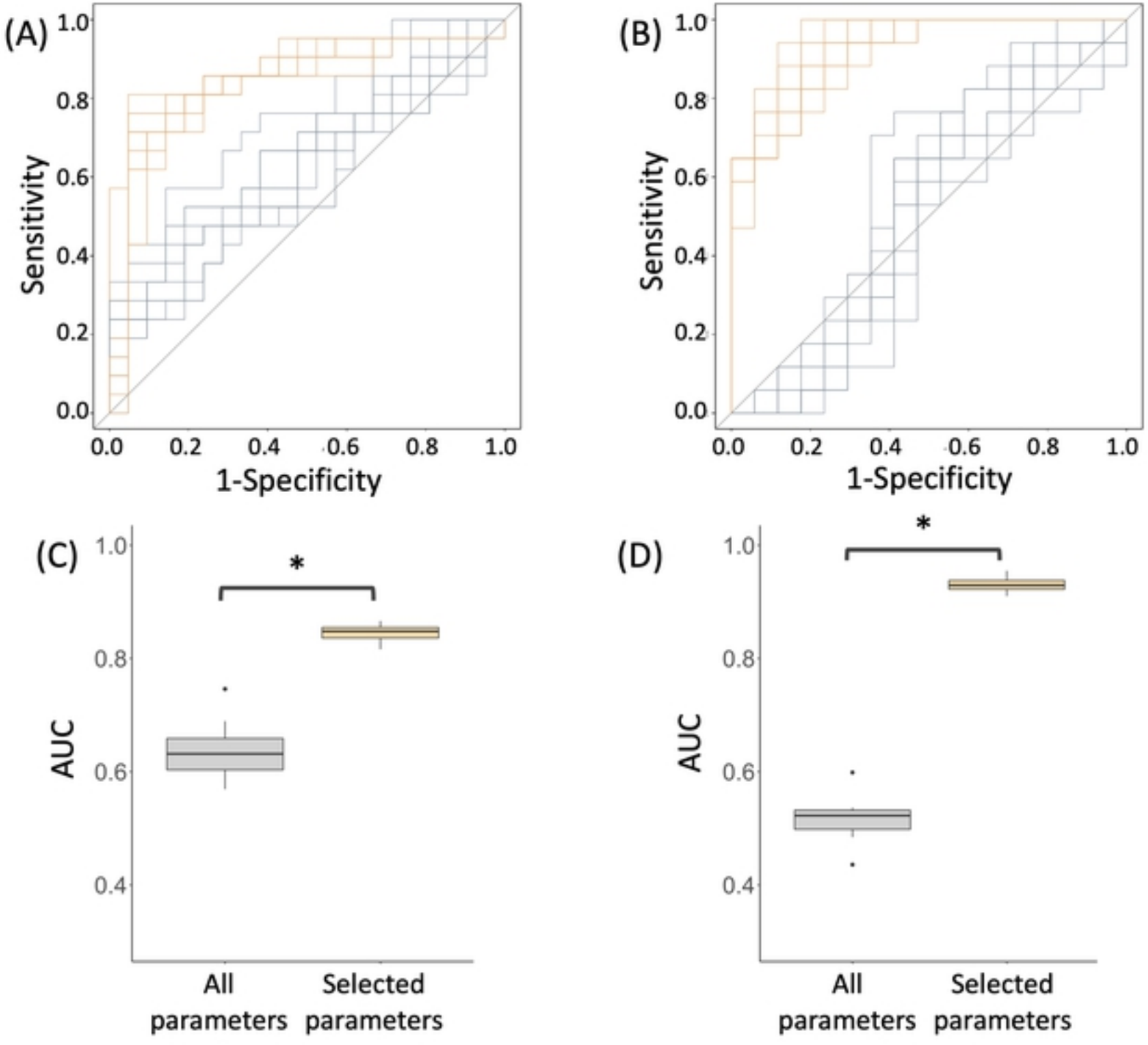

Oka et al. Figs. 3A to 3D

Figure

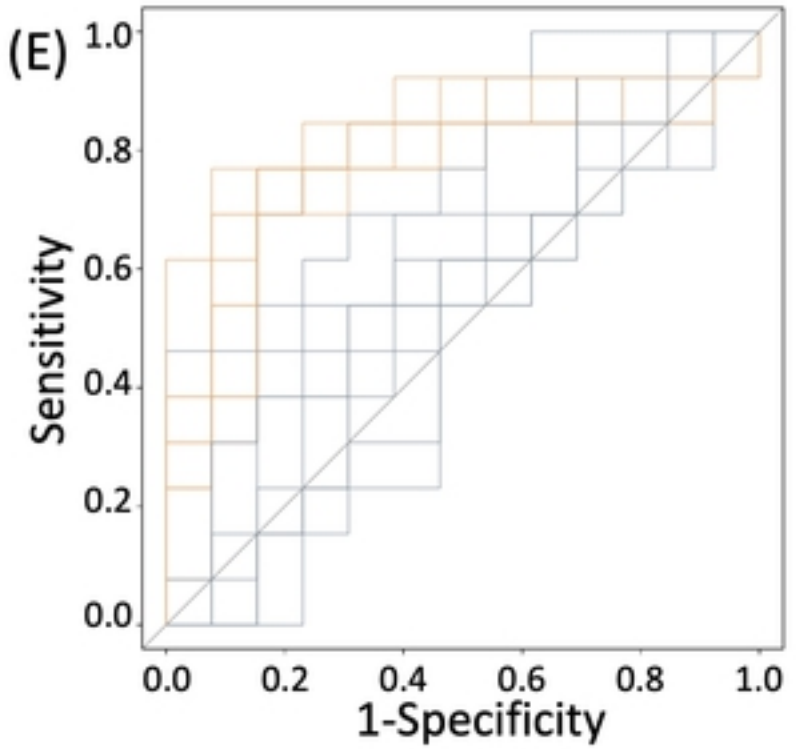

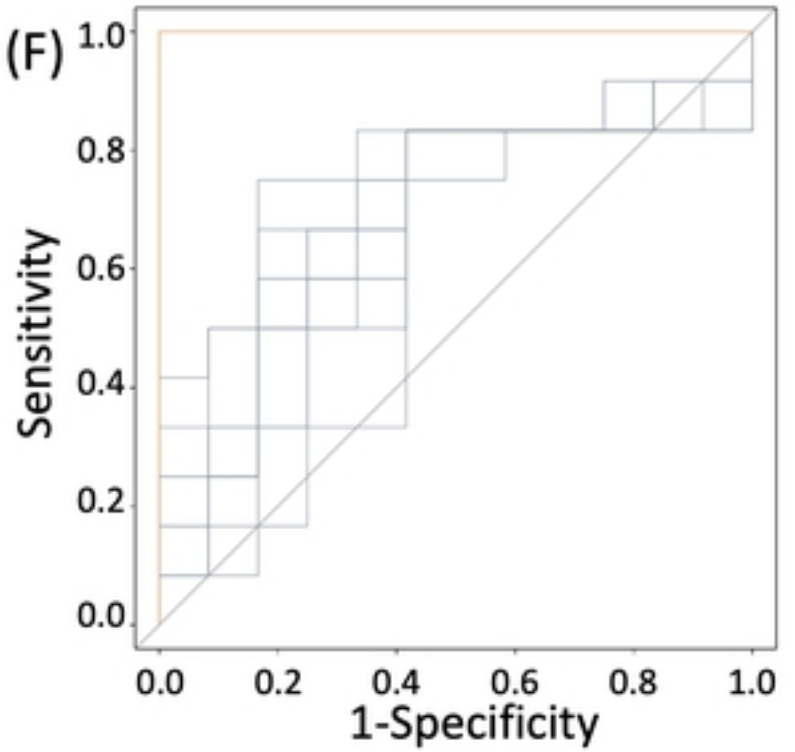

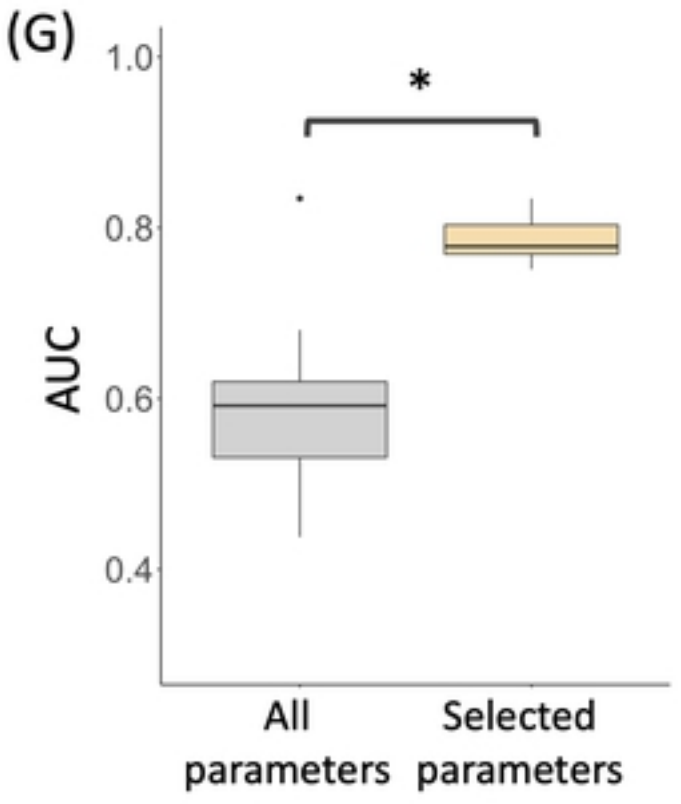

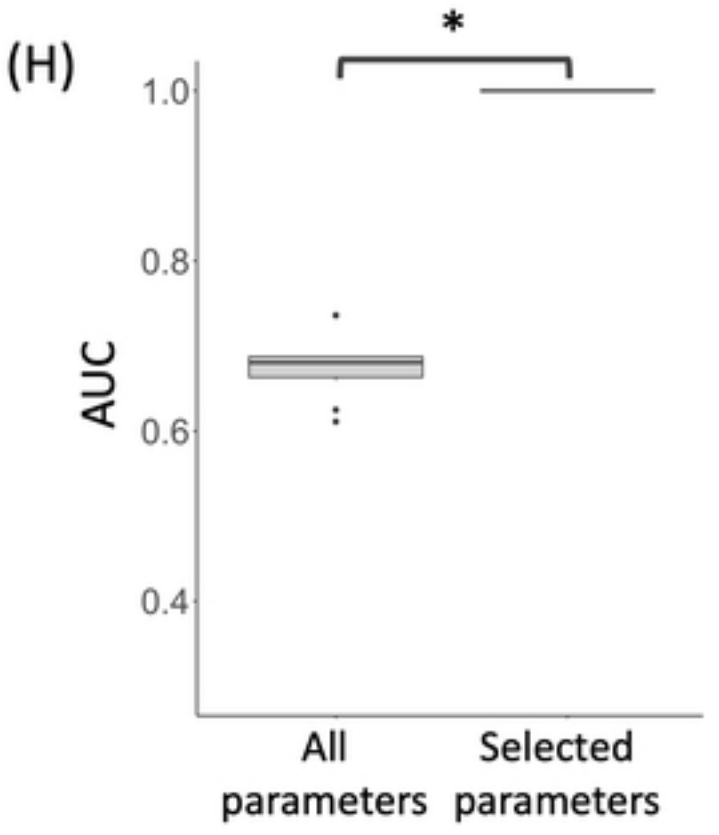

All parameters

Selected parameters

* : p-value < 0.05

All parameters

Selected parameters

Oka et al. Figs. 3E to 3H

Figure